



HAL
open science

**Structures of $[M(\text{Ura-H})(\text{Ura})]^+$ and
 $[M(\text{Ura-H})(\text{H}_2\text{O})_n]^+$ ($M = \text{Cu, Zn, Pb}$; $n = 1-3$)
complexes in the gas phase by IRMPD spectroscopy in
the fingerprint region and theoretical studies**

Barry Power, Violette Haldys, Jean-Yves Salpin, Travis D Fridgen

► **To cite this version:**

Barry Power, Violette Haldys, Jean-Yves Salpin, Travis D Fridgen. Structures of $[M(\text{Ura-H})(\text{Ura})]^+$ and $[M(\text{Ura-H})(\text{H}_2\text{O})_n]^+$ ($M = \text{Cu, Zn, Pb}$; $n = 1-3$) complexes in the gas phase by IRMPD spectroscopy in the fingerprint region and theoretical studies. *International Journal of Mass Spectrometry*, 2018, 429, pp.56 - 65. 10.1016/j.ijms.2017.05.003 . hal-01889158

HAL Id: hal-01889158

<https://hal.science/hal-01889158>

Submitted on 8 Oct 2018

HAL is a multi-disciplinary open access archive for the deposit and dissemination of scientific research documents, whether they are published or not. The documents may come from teaching and research institutions in France or abroad, or from public or private research centers.

L'archive ouverte pluridisciplinaire **HAL**, est destinée au dépôt et à la diffusion de documents scientifiques de niveau recherche, publiés ou non, émanant des établissements d'enseignement et de recherche français ou étrangers, des laboratoires publics ou privés.

**Structures of $[M(\text{Ura-H})(\text{Ura})]^+$ and $[M(\text{Ura-H})(\text{H}_2\text{O})_n]^+$ ($M = \text{Cu}$,
 Zn , Pb ; $n = 1 - 3$) Complexes in the Gas Phase by IRMPD
Spectroscopy in the Fingerprint Region and Theoretical Studies**

Barry Power,^a Violette Haldys,^{b,c} Jean-Yves Salpin,^{b,c} and Travis D. Fridgen^a

a: Department of Chemistry, Memorial University, St. John's, NL, A1B 3X7, Canada.

b: LAMBE, Université Evry Val d'Essonne, CEA, CNRS, Université Paris-Saclay, F-91025, Evry,
France

c LAMBE, Université Cergy-Pontoise, Université Paris-Seine, F-91025, Evry, France

Abstract

The gas-phase structures of the bare dimers, $[M(\text{Ura-H})(\text{Ura})]^+$, and hydrated monomers, $[M(\text{Ura-H})(\text{H}_2\text{O})_n]^+$, were examined using infrared multiple photon dissociation spectroscopy in the fingerprint region ($1000\text{ cm}^{-1} - 1900\text{ cm}^{-1}$) for $M = \text{Cu}, \text{Zn},$ and Pb and $n = 1 - 3$. The experimental results were compared to those calculated using density functional methods. The dimeric structures all show deprotonation of one uracil moiety at N3, and forms a tetracoordinate interaction with N3 and O4 of the deprotonated uracil, and N3 and O2 of the neutral uracil. The hydrated monomers, $[M(\text{Ura-H})(\text{H}_2\text{O})]^+$, all have rather different structures. Uracil is deprotonated at N3 for $M = \text{Zn}$ and Pb , but for Cu , uracil is deprotonated at N1 and Cu^{2+} is bound to N1 and O2. Like the $[M(\text{Ura-H})(\text{Ura})]^+$ complexes, in $[\text{Pb}(\text{Ura-H})(\text{H}_2\text{O})]^+$ the metal is bound to N3 and O4. The Zn^{2+} complex actually better resembles $[M(\text{Ura})(\text{OH})]^+$ with a proton apparently transferred from water to O4 of uracil and the metal cation coordinated to O2. Unlike the singly hydrated complex, uracil is deprotonated at N3 in $[\text{Cu}(\text{Ura-H})(\text{H}_2\text{O})_2]^+$. In all singly, doubly, and triply solvated complexes studied, water is found to be coordinated to the metal cation.

1. Introduction

The sequencing of nucleobases in DNA and RNA forms the basis of our genetic code. The formation of proteins relies upon proper transcription of the DNA sequence to messenger RNA, through the Watson-Crick pairing of nucleobases [1]. This proper base pairing is dependent upon hydrogen bonding interactions. Should the configuration of a nucleobase be altered, resulting in changes to hydrogen bonding sites, disruption of proper Watson-Crick pairing can result, leading to errors in transcription and thus genetic mutations. Among other biological processes, metal ions play an important role in RNA stability and activity [2–4], but their presence also has the ability to affect the tautomerization of nucleobases [5], thus impacting the hydrogen bonding sites and potentially leading to mis-matched base pairs and genetic mutations [6]. Transition metal dications have shown an increased affinity towards nucleobases compared to their group 2 counterparts [7], with copper having the greatest affinity of the divalent cations [8]. Cu^{2+} is one of the metal ions of interest in this current work, along with Zn^{2+} and Pb^{2+} , and the impact they have on the structure of both bare and hydrated uracil complexes.

Each of these metals has been thoroughly explored in terms of their enhancement of or interference in biological processes. While copper is important to nucleotide stability, it can also reach toxic levels in cells, causing reduction of hydrogen peroxide in the mitochondria. As a result, this produces highly reactive hydroxyl radicals which can negatively impact DNA and cause membrane damage [9,10]. Zinc is one of the most abundant d-block elements found in cell cytoplasm, and has a role in gene regulation and protein folding [11,12], making its inclusion in this work particularly interesting. The toxic impact and detrimental effect Pb^{2+} has on human health has been well documented, in particular its disruption of biological homeostasis and its targeting of the heart, liver and kidneys [13].

While several stable tautomers of uracil exist, as well as its DNA replacement thymine, it is the diketo form that is favoured [14–18]. The diketo tautomer of uracil, along with the numbering scheme for uracil, is presented in Scheme 1. The interaction of the Cu^{2+} , Zn^{2+} and Pb^{2+} ions with both uracil and thymine have been explored both experimentally and computationally. Both Cu^{2+} and Zn^{2+} have been shown to stabilize the keto-enol tautomer of thymine [19]. When complexed with uracil, each of these dications will deprotonate uracil to form a singly charged ion of the form $[\text{M}(\text{Ura-H})]^+$. However, the site of deprotonation is dependent upon the metal. Both Pb^{2+} [20] and Zn^{2+} [21] will deprotonate uracil from the N3 position, and form a bidentate interaction with uracil at N3 and O4. This binding is also characteristic of the $[\text{M}(\text{Ura-H})]^+$ moiety in $[\text{M}(\text{Ura-H})(\text{Ura})]^+$ (loosely termed “dimeric complex”) when M is Zn or Pb [22,23] or the group 2 cations [24–26]. By contrast, the $[\text{Cu}(\text{Ura-H})]^+$ complex was shown to be deprotonated at the N1 position of uracil, with Cu bound to N1 and O2 [27,28]. However, the dimeric complex adopts a similar structure to the Pb and Zn dimers, where deprotonation occurs at N3 and metal binding is to N3 and O4 of the deprotonated moiety [23,29,30].

The current work uses IRMPD spectroscopy in the fingerprint region ($1000\text{ cm}^{-1} - 1900\text{ cm}^{-1}$) to explore the structures of bare dimeric $[\text{M}(\text{Ura-H})(\text{Ura})]^+$ complexes, as well as hydrated monomers $[\text{M}(\text{Ura-H})(\text{H}_2\text{O})]^+$, where M = Cu, Zn, and Pb. The doubly hydrated monomers of Cu and Zn are also examined, along with the triply hydrated Zn monomer. The chief feature in the fingerprint region is carbonyl stretching, which is then compared to the computed spectra for several lowest energy isomers for each complex.

2. Methods

2.1. Experimental

All experiments were performed using a Fourier-transform ion cyclotron resonance mass spectrometer (FT-ICR-MS) coupled to a mid-infrared free electron laser (FEL) at the Centre Laser Infrarouge d'Orsay (CLIO) [31,32]. 0.01 mmol L⁻¹ solutions of the chloride salts of each metal ion were prepared using 18 MΩ-cm water (Millipore). Uracil solutions were prepared to 1 mmol L⁻¹ in 18 MΩ-cm water (Millipore). Mixtures were then prepared in a 1 to 10 ratio of metal solution to uracil solution, and introduced via syringe injection to the electrospray ion source at a flow rate of 75 μL h⁻¹. The ions were mass selected with a quadrupole mass filter and introduced in to the ICR cell, where they are then isolated and irradiated with the free electron laser. To accomplish hydration, bare [M(Ura-H)]⁺ ions were mass selected in the quadrupole mass filter and stored in the hexapole storage cell, where water vapour had been introduced [33]. Irradiation times varied from 0.1 to 3 s, with the shorter irradiation times corresponding to the more weakly bound hydrated ions. Areas of the IRMPD spectra which experienced saturation were scanned after attenuation of the FEL. The laser was scanned at 5 cm⁻¹ intervals from ~1000 to 1900 cm⁻¹. The IRMPD efficiency is the negative of the natural logarithm of parent ion intensity divided by the sum of parent and fragment ion signals.

2.2. Computational

Calculations for all structures were conducted using the Gaussian 09 suite of programs [34]. Each structure was optimized, and infrared spectra computed, using B3LYP density functional theory. For the complexes of Cu and Zn, the 6-31+G(d,p) basis set was applied to all atoms. For complexes of Pb, the LANL2DZ basis set with relativistic core potential was applied

to the Pb atom and the 6-31+G(d,p) basis was used for all other atoms. Single point energy calculations were then carried out using B3LYP with the 6-311+G(3df,3pd) basis set on all atoms except Pb, for which the LANL2DZ basis set with relativistic core potential was used. This computational method will be referred to as method 1.

All calculations were then repeated, for the five lowest energy structures, with the def2-TZVPP basis set which has been found to work better for metal-cation amino acid complexes than the LANL2DZ [35,36] for all metals during both the optimization and single point energy calculations. The def2-TZVPP basis set contains polarization functions, which are not included in the LANL2DZ basis set. The 6-31+G(d,p) basis set was again used for all other atoms (C, H, N and O) during optimization, followed by the 6-311+G(3df,3pd) basis set for single point energy calculations. This computational method will be referred to as method 2.

These single-point electronic energies, using methods 1 and 2 were used to compute the enthalpies and Gibbs energies of isomeric species at 298 K, using the unscaled harmonic vibrational frequencies calculated for the optimization geometries.

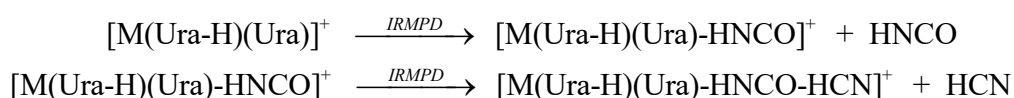
The bonding within the individual equilibrium structures was also explored by locating the bond critical points (BCPs) using atoms-in-molecules (AIM) theory [37], which is based on a topological analysis of the electronic density at the BCPs, and is a good descriptor of the bond character; electrostatic or covalent. This analysis was conducted using optimized structures from method 2 using the AIMAll software [38]. Data from the topological analysis are given collectively in the Supporting Information as Figure S12.

For comparison with the experimental spectra, the computed infrared spectra were all scaled by a factor of 0.97 and convoluted with a Lorentzian profile with a width (FWHM) of 15 cm^{-1} .

3. Results and Discussion

3.1. Examination of the IRMPD Spectra

For the hydrated monomers of all metals, the primary fragmentation pathway results from the sequential loss of water solvent molecules. For the case of the bare dimer complexes, the primary fragmentation pathway is dependent upon the identity of the metal center [22,23,29]. For $M = \text{Cu}$ and Zn ,



where the identity of the fragment ions for the Cu^{2+} complex was explored previously [29]. $[\text{Pb}(\text{Ura-H})(\text{Ura})]^+$ simply loses uracil upon IRMPD activation. The hydrated complexes were found to simply lose solvent.

Figure 1 is a comparison of the experimental spectra for all $[\text{M}(\text{Ura-H})(\text{Ura})]^+$ complexes in the $1000 - 1900 \text{ cm}^{-1}$ region. All three complexes exhibit similar features in the $1517 - 1553 \text{ cm}^{-1}$ region, corresponding to an enolic C–OH stretch, characteristic of the lowest energy structures of each which will be discussed later. Above 1600 cm^{-1} , only one band is observed for the Zn and Pb complexes, while two major bands are observed in the Cu complex. For the Cu complex, blue shifting of the C=O stretch, by approximately $60 - 70 \text{ cm}^{-1}$ in comparison to the other metals, allows the intense C=C stretch (1626 cm^{-1}), and the carbonyl stretches centered at 1678 cm^{-1} to be resolved. This separation is not seen in the Zn and Pb complexes, as one broad band encompasses both the C=C and C=O stretching modes. For the Cu^{2+} complex, a slight distinction between the different carbonyl stretching modes is observed, with the metal coordinated carbonyl stretch emerging as a shoulder on the red side of this band. The carbonyl stretching bands, for all complexes, are red-shifted in comparison to the free C=O stretch of uracil, at 1750 cm^{-1} in the gas phase [39], as metal coordination weakens the carbonyl bond. When compared to

the $[M(\text{Ura-H})(\text{Ura})]^+$ complexes of group 2 dications, these carbonyl stretches occur in roughly the same position [25], with the exception of the Cu^{2+} complex. The blue-shifting of the carbonyl stretches of the $[\text{Cu}(\text{Ura-H})(\text{Ura})]^+$ complex in comparison to the other metals is rationalized in the following way; It has previously been demonstrated that Cu^{2+} exhibits greater binding energy to carbonyl groups of peptide ligands [40]. Though this would intuitively suggest a weakening of the carbonyl bond, metal-to-ligand charge transfer is facilitated as a result of this increased binding energy, donating electron density back to the carbonyl, which serves to strengthen the carbonyl bond. It would be reasonable to expect a similar result in the present complexes.

For the bare monomeric species, $[M(\text{Ura-H})]^+$, an IRMPD spectrum has been recently obtained for $M = \text{Pb}$ [41] by coupling the FEL to a quadrupole ion trap. For this complex, Pb interacts with uracil at the O4 carbonyl [20], and a very intense signal at 1755 cm^{-1} corresponds to the free carbonyl stretch at O2. Consequently, the free C=O stretch can result in a very intense feature under IRMPD conditions. Within this current work, IRMPD spectra could not be obtained for the $[M(\text{Ura-H})]^+$ complexes, presumably because the dissociation energy was too high to be reached under our experimental conditions.. However, the solvated monomers are easily dissociated and were examined using IRMPD spectroscopy. In Figure 2, the IRMPD spectrum for the $[M(\text{Ura-H})(\text{H}_2\text{O})]^+$ complexes in the $1000 - 1900 \text{ cm}^{-1}$ region are presented. The spectrum of the $[\text{Pb}(\text{Ura-H})(\text{H}_2\text{O})]^+$ complex offers many distinct features to assist in characterization, such as the carbonyl stretch (centered at 1702 cm^{-1}), C=C stretching and H_2O scissoring (1595 cm^{-1}), metal coordinated carbonyl stretch (1534 cm^{-1}) and N-H wagging (1454 cm^{-1}). An additional signal is also observed around 1750 cm^{-1} , in the area of a free carbonyl stretch. The spectrum for Cu contains a band in the carbonyl stretching region, although it is significantly red-shifted in comparison to the Pb spectrum. Aside from that, there is a large, broad absorption between 1400

cm^{-1} and 1550 cm^{-1} . Interestingly, the spectrum for $[\text{Zn}(\text{Ura-H})(\text{H}_2\text{O})]^+$ shows no features above 1600 cm^{-1} , only an intense band at 1588 cm^{-1} and a broad feature centred at 1486 cm^{-1} . The intense band is in the C=C and red-shifted C=O stretching regions, while the 1486 cm^{-1} feature is in the protonated carbonyl stretching region.

Figure 3 shows the IRMPD spectrum for the doubly and triply hydrated monomers in the fingerprint region. An experimental spectrum for $[\text{Pb}(\text{Ura-H})(\text{H}_2\text{O})_2]^+$ could not be obtained due to the inability to isolate enough of the ion, and only the triply hydrated Zn species was isolated. Neither of the spectra for the doubly or triply hydrated Zn^{2+} complexes offer much in the way of band resolution, although broad absorptions with a sharp onset at about 1720 cm^{-1} are observed down to about 1375 cm^{-1} . The $[\text{Cu}(\text{Ura-H})(\text{H}_2\text{O})_2]^+$ complex, on the other hand, gives a very well resolved spectrum with bands at 1712 cm^{-1} (carbonyl stretching), 1602 cm^{-1} (H_2O scissoring), 1533 cm^{-1} (C=C/C=O stretching) and 1454 cm^{-1} (N-H wagging). As noted above, the carbonyl stretching is shown to be higher in energy when Cu is the metal center, but the inclusion of two water molecules leads to donation of electron density back to the carbonyl bonds, strengthening them even further, which blue-shifts this carbonyl stretch even more.

3.2. Computed Structures for $[\text{M}(\text{Ura-H})(\text{Ura})]^+$

A total of 27 minima were found for the Cu^{2+} complex, 25 for the Zn^{2+} complex and 16 for the Pb^{2+} complex. In Figure 4, the geometries and energetics for the lowest energy isomers of each complex are presented, based upon the results of calculation method 2. In Figures S1 to S3 (Supporting Information), all structures and energetics are presented for the method 1, along with a comparison of energetics by method 2 for the five lowest energy structures, where relatively good agreement is noted across both methods. In the isomer labelled as structure i in Fig. 4, one

uracil is deprotonated at N3, and metal coordination occurs between N3 and O4. The neutral uracil is a tautomer where hydrogen has been transferred from N3 to O4, and the metal is coordinated to N3 and O2. An intramolecular hydrogen bond occurs between the O4 enol of the neutral uracil and O2 carbonyl of the deprotonated uracil. With a bond length of ~ 1.5 Å, this interaction is relatively strong. This isomer is the lowest in energy for the M = Cu and Pb complexes, which is consistent with results previously obtained for Cu [23,29] and Pb [22], and comparable to the ammoniated dimer of Cu [30] as well as similar bare dimers metalated by group 2 dications [24,25]. This structure is only slightly higher in energy for the Zn complex by a nominal amount.

AIM topological analysis (Supporting Information, Fig. S12) was conducted for isomer i for each complex, as well as isomer ii for the Zn complex, which is lowest in energy for that metal. The tetradentate metal interactions are confirmed by the topological analysis, as four bond critical points (BCPs) are observed connecting the metal to the two uracil units. The metal-uracil and hydrogen bonding interactions are electrostatic as indicated by the positive values of the Laplacian of the electron density, $\nabla^2\rho$, (Supporting Information, Fig. S12). The free carbonyl is the shortest of all C=O bonds, followed by the metal coordinated carbonyls and then the protonated carbonyl C=O bond. In terms of the two metal coordinated carbonyls, that of the deprotonated uracil is slightly longer.

These structural differences away from the neutral diketo tautomer, as a result of the presence of the metal ion, can have biological impacts through the disruption of hydrogen bonding between base pairs [42–44]. Both the deprotonation as well as the keto-enol proton transfer change the hydrogen bonding environment and may have a negative effect on the structural integrity of the nucleic acid strand, specifically RNA in the case of uracil.

Two additional structures in Figure 4 found to be comparable in terms of energy show only slight differences from the first structure. In structure ii, the metal is coordinated to the N3 and O4 of the uracil where the proton has been transferred to O2, and an intermolecular hydrogen bond is formed between O2 enol of uracil, and O2 of deprotonated uracil. This particular structure is the lowest in energy when Zn is the metal center. Structure iii instead has metal coordination to N3 and O2 of both uracils, proton transfer from N3 to O4, and an intermolecular hydrogen bond between the O4 enol and the O4 of deprotonated uracil. Specific to the Pb complex is a fourth structure nearly identical to the first, labelled as structure iv. In this configuration, Pb is coordinated at the N3 and O2 position of deprotonated uracil, and N3 and O4 of the neutral uracil where proton transfer from N3 results in a tautomer with an enol at O2. This enol then hydrogen bonds to the O4 of the deprotonated uracil. This particular isomer is observed using method 1 for Zn, but optimizes to give the structure i using method 2, as the enol proton is transferred between uracil moieties. When Cu is the metal center, this configuration optimizes as structure i for both calculation methods. All other isomers were determined to be significantly higher in energy by both methods of calculation.

All lowest energy structures are planar for Cu and Zn, but are bent for Pb at an angle of approximately 125°. This is to be expected, given the much larger size of the Pb ion in combination with repulsion from the lone pair of electrons in a hybridized sp orbital.

3.2.1. Comparison of Computed and Experimental Spectra

A comparison of the experimental spectra for the $[M(\text{Ura-H})(\text{Ura})]^+$ structures with the calculated spectra for isomers i – iv is shown in Figure 5. For each metal, structure i seems to offer the best agreement with the experimental spectra. In the Cu^{2+} complex, the bands above

1600 cm^{-1} are resolved, which contrasts with the Zn and Pb complexes. This resolution offers three distinct maxima – a band centered at 1678 cm^{-1} with a shoulder at 1663 cm^{-1} (hydrogen bonded and metal coordinated carbonyls, respectively), and another band at 1626 cm^{-1} , reflective of the C=C stretch. Each of these vibrations are observed in the computed spectrum for structure i, although a large, unresolved band in this area appears for structure iii which cannot be discredited. Perhaps the most distinguishing feature is the less intense protonated C=O stretch at 1553 cm^{-1} in the experimental spectrum, which only occurs in structure i.

In the experimental IRMPD spectra for Zn^{2+} and Pb^{2+} complexes, the same resolution in the C=O and C=C region is not observed as it was for the Cu^{2+} complex. The calculated spectra for structure i does differentiate between these stretches, with the hydrogen bonded carbonyl, $\sim 1670 \text{ cm}^{-1}$, appearing to the blue of the metal coordinated carbonyl band, which is the one corresponding to the experimental spectrum. In the experimental spectrum of the Zn complex, a very weak feature is observed that corresponds to the calculated position of the hydrogen bonded carbonyl stretch by structure i. The protonated C=O stretches, however, exhibit good agreement between experimental and structure i. Given the lack of resolution between carbonyl stretches in experimental spectra, which is more consistent with structure iii, no definitive assignment can be made to the primary contributing structure for the Zn and Pb dimers. Structure ii, which is actually lowest in energy for the Zn complex, could also be considered although it offers resolution of all carbonyl and C=C stretches which was not observed experimentally.

3.3. Computed Structures for $[\text{M}(\text{Ura-H})(\text{H}_2\text{O})]^+$

There are 7 different isomers obtained for the $[\text{Pb}(\text{Ura-H})(\text{H}_2\text{O})]^+$ complex, along with 25 for Zn and 19 for Cu by computational method 1. These structures, along with energetics, are

presented in Figures S4 to S6 (Supporting Information), along with a comparison of the computed relative energetics to method 2 for the five lowest energy structures. Once again, good agreement is obtained across both methods. The lowest energy structures were re-optimized using method 2 and are summarized in Figure 6. The structures of $[\text{Pb}(\text{Ura-H})(\text{H}_2\text{O})]^+$ are consistent with those calculated previously [22], in which the lowest energy structure is deprotonated at the N3 position, Pb coordinates to N3 and the O4 carbonyl, and the water molecule is bound directly to the Pb center with a hydrogen bonding interaction to the O2 carbonyl. This structure is identified as 1-i(Pb). Through the AIM topological analysis (Supporting Information, Fig. S12), the electrostatic nature of this bidentate interaction is confirmed, as is the hydrogen bonding relationship. A second structure just slightly higher in energy, 1-ii(Pb), once again demonstrates deprotonation at N3 and water coordination directly to Pb, but now shows Pb coordination to N3 and O2, with water hydrogen bonding to the O4 carbonyl. For both isomers, the carbonyl involved in metal coordination is consistently longer ($\sim 1.26 \text{ \AA} - 1.27 \text{ \AA}$) than the other carbonyl bond ($\sim 1.24 \text{ \AA} - 1.25 \text{ \AA}$), although this discrepancy in bond lengths is much larger in structure 1-i(Pb).

Given the lack of a carbonyl feature in the experimental spectrum for $[\text{Zn}(\text{Ura-H})(\text{H}_2\text{O})]^+$, additional structures were optimized in which the water solvent transfers a proton to the uracil moiety, resulting in a $[\text{Zn}(\text{Ura})(\text{OH})]^+$ complex. This particular configuration proved to be lowest in energy. Deprotonation is again at the N3 position. One would expect a bidentate interaction of Zn with the N3 and O2 positions, however the AIM analysis indicates there is only a single interaction between Zn and O2, with no BCP present between Zn and N3. Proton transfer apparently occurs from water to O4, resulting in a neutral keto-enol tautomer of uracil. The resulting hydroxide is bound directly to Zn, and does not participate in any hydrogen bonding interactions with the uracil moiety. As this structure is a keto-enol tautomer, the carbonyl bond

lengths are notably longer, at 1.31 Å for the enol and 1.28 Å for the metal coordinated carbonyl. A similar structure just slightly higher in energy has Zn coordination to O4, with a proton transferred from water to the O2 position, resulting in an enol. It has been shown that water bound to Zn^{2+} experiences a decrease in pK_a from 15.7 to 7.9 [45], facilitating the loss of a proton from water. The deprotonation of water by Zn^{2+} has been observed previously, particularly in metalloenzymes. Zn^{2+} has a d^{10} configuration, and thus is not subject to ligand field stabilization effects, making it suitable for interaction with protein-binding sites that deviate from an octahedral geometry or coordination number of 6 [45], nor is it capable of any redox activity. In carbonic anhydrase, zinc-bound hydroxide attacks CO_2 to form zinc-bound bicarbonate, and the bicarbonate is subsequently replaced by a water molecule. The water molecule very rapidly ionizes to regenerate zinc-bound hydroxide, a process facilitated by histidine-64, where the proton is shuttled to the non-hydrogenated imidazole nitrogen [45]. The $[\text{Zn}(\text{Ura-H})(\text{H}_2\text{O})]^+$ isomers where the water molecule remain intact are $> 25 \text{ kJ mol}^{-1}$ higher in energy.

In the case of $[\text{Cu}(\text{Ura-H})(\text{H}_2\text{O})]^+$, the lowest energy structure is deprotonated at the N1 position, similar to the bare monomer. Much like the Zn complex, there is seemingly a bidentate interaction with copper coordinated to the N1 and O2 position, however the AIM topological analysis does not show a BCP between Cu and O2. The water molecule, bound directly to Cu, does not interact with the uracil moiety. This structure is labelled as 1-i(Cu) in Fig. 6. Now that both carbonyl bonds are free, they display a similar length at $\sim 1.22 \text{ \AA}$. Even though the 1-i(Cu) structure is lowest in energy, the N3 deprotonated structure, 1-ii(Cu), is now relatively closer in terms of energy when compared to the bare structures, which were separated by approximately 15 – 35 kJ mol^{-1} [27,29]. Considering that these two bare monomers were virtually isoenergetic when

solvent model calculations were performed [29], one would expect that the inclusion of solvent molecules would close the gap in energy between the N1 and N3 deprotonated structures.

3.3.1. Comparison of Computed and Experimental Spectra for $[\text{Zn}(\text{Ura-H})(\text{H}_2\text{O})]^+$ and $[\text{Pb}(\text{Ura-H})(\text{H}_2\text{O})]^+$

A comparison of the experimental spectra for the $[\text{M}(\text{Ura-H})(\text{Ura})]^+$ structures with the calculated spectra for isomers 1-i – 1-iii is shown in Figure 7. For the Zn complex, good agreement is observed between the experimental spectrum and the calculated spectra for each of the three lowest energy isomers. Structure 1-i(Zn) is the best match with the experimental spectrum in terms of both band shape and position, although neither 1-ii(Zn) nor 1-iii(Zn) can be discounted entirely. The intense band at 1588 cm^{-1} in the experimental spectrum, a combination of both metal coordinated carbonyl and C=C stretching, is observed at 1611 cm^{-1} for isomer 1-i(Zn). These two modes are separated in isomer 1-ii(Zn) and is red-shifted to 1628 cm^{-1} in structure 1-iii(Zn). The protonated C=O stretch experimentally observed at 1486 cm^{-1} occurs at 1492 cm^{-1} in isomer 1-i(Zn), demonstrating remarkable agreement. Congruence is also noted at the enlarged feature at 1175 cm^{-1} , where both C-H wagging and enolic O-H wagging occur.

In previous work involving the Pb complex, both structure 1-i and 1-ii were identical to the experimental spectrum in the O-H/N-H region, and could not be distinguished from one another [22]. With the current work in the mid-infrared region, differences between the calculated spectra of these isomers are observed, and structure 1-i corresponds most closely with the experimental spectrum. In particular, there is good alignment with all features below 1550 cm^{-1} , namely the metal coordinated carbonyl (1534 cm^{-1}) and N-H wagging (1454 cm^{-1}), along with the more minor features of C-N stretching at 1360 cm^{-1} and C-H wagging at 1190 cm^{-1} . The most predominant

feature in the experimental spectrum, an intense band with a maximum at 1595 cm^{-1} with a shoulder to the blue, aligns closely with the two better-resolved bands in the spectrum for 1-i, attributed to H_2O scissoring, at the lower frequency, and $\text{C}=\text{C}$ stretching. The carbonyl stretch is in a position slightly lower in frequency in the calculated spectra for structure 1-i, at 1684 cm^{-1} , however it offers the closest agreement with the experimental carbonyl stretch of all computed structures. Structure 1-ii cannot be ignored entirely as a contributor, especially considering the good agreement in the most intense band at 1595 cm^{-1} , in addition to a small band at 1660 cm^{-1} in the experimental spectrum, between two far more intense bands which is in good agreement with the carbonyl stretch of structure 1-ii. Finally, note that an experimental signal is also observed around 1750 cm^{-1} . Comparison with the IRMPD spectrum obtained for the $[\text{Pb}(\text{Ura-H})]^+$ complex [41] suggests that this experimental feature probably corresponds to the stretching of a free $\text{C}=\text{O}$ group. This signal proves to be in good agreement with the free $\text{C}=\text{O}$ stretch computed for the 1-iii structure, which is located only 11.1 kJ mol^{-1} higher in Gibbs energy. Therefore, a mixture of at least two different forms may be obtained for the $[\text{Pb}(\text{Ura-H})(\text{H}_2\text{O})]^+$ complex, with a minor contribution of 1-iii as suggested by the weak abundance of the experimental signal. Note that the bond length computed for the O_2 carbonyl in 1-iii (1.215 \AA) is similar to the bond length obtained for the $[\text{Pb}(\text{Ura-H})]^+$ ion (1.213 \AA), consistent with a similar position of the experimental band.

3.3.2. Spectra for $[\text{Cu}(\text{Ura-H})(\text{H}_2\text{O})]^+$

The singly hydrated monomer of Cu presents a perplexing result when compared to the experimental spectrum, where neither of the calculated spectra is in good agreement. The calculated spectra for structures 1-ii and 1-iii are nearly identical, as the structures differ only by rotation in the water molecule. Based on the lowest energy structures, the free carbonyl stretching should be readily observed, a feature that is present experimentally, but is not as intense as one

would expect from the computed spectra. A minor band observed experimentally 1712 cm^{-1} does offer agreement with the band observed for structure 1-i corresponding to the O2 carbonyl stretch. The sharpest and most intense band in the experimental spectrum is 1621 cm^{-1} , and one broad band covering the area from 1400 cm^{-1} to 1550 cm^{-1} , neither of which can be accounted for in the spectra in the lowest energy structures.

The number of initial input geometries used to determine the lowest energy structure through calculations was greatly expanded for these complexes, although a lower energy isomer was not found. Isomers having the form $[\text{Cu}(\text{Ura})(\text{OH})]^+$, the configuration adopted by the Zn complex, were also explored resulting in 13 additional structures, none of which were lower in energy than structure 1-i(Cu) by calculation method 1. A comparison of these structures is presented in Figure S10 of the Supporting Information. Solvent modelling as well as an empirical dispersion correction were both added to the $[\text{Cu}(\text{Ura-H})(\text{H}_2\text{O})]^+$ complexes when calculating in an effort to find another structure lower in energy that may match the experimental spectra, but to no avail. Although the experimental spectra in the high frequency O-H/N-H stretching region has not been collected, a comparison of the calculated spectra in this region for the three lowest energy structures (Supporting Information, Figure S11) suggests that this region would not offer any useful information in terms of complex determination, as the calculated spectra are all identical.

3.4. Computed Structures for $[\text{M}(\text{Ura-H})(\text{H}_2\text{O})_2]^+$

For the doubly hydrated monomers, only calculations of the Cu and Zn species were conducted since the Pb complex was not observed experimentally. For the Cu complex, a total of 57 isomers were optimized by method 1, along with 39 distinct isomers of the Zn complex. All of these isomers are given in Figures S7 and S8 (Supporting Information), along with a comparison of energetics to method 2 for the five lowest energy structures. The calculations were repeated on

the lowest energy structures using method 2, with the results presented in Figure 8 along with the calculated energetics and spectra.

For $[\text{Cu}(\text{Ura-H})(\text{H}_2\text{O})_2]^+$, the inclusion of a second water molecule leads to the lowest energy structure now exhibiting deprotonation at N3, with Cu coordinated to N3 and O4, and two solvent molecules are bound directly to Cu. One of these water molecules participates in a hydrogen bond with the O2 carbonyl, which is not involved in metal binding. This isomer is referred to as 2-i. This presents a noticeable change in structure in comparison to the bare $[\text{Cu}(\text{Ura-H})]^+$ [27], as well as the structure currently determined as lowest in energy for $[\text{Cu}(\text{Ura-H})(\text{H}_2\text{O})]^+$, both of which are deprotonated at the N1 position, demonstrating a clear solvent effect. Structure 2-iii is opposite in terms of the behaviour of the carbonyl groups, with the metal now bound to N3 and O2, two water molecules bound directly to Cu, one of which interacting with O4 through hydrogen bonding. The middle isomer, structure 2-ii, is interesting in that there is no bidentate interaction between Cu and uracil. Rather, Cu is bound only to the deprotonated N3 position. Both water molecules are still coordinated directly to Cu, which is common to all isomers. However, since neither carbonyl interacts with the metal ion, they are both available for hydrogen bonding with the solvent. When using structures 2-i, 2-ii and 2-iii as the initial input for optimization calculations for $[\text{Zn}(\text{Ura-H})(\text{H}_2\text{O})_2]^+$, each results in the 2-ii isomer, which is significantly lower in energy than any other isomer. It is interesting to note that the Zn complex prefers the configuration where the metal has just a single interaction with uracil. However, the characteristics of N3 deprotonation and solvent coordination directly to the metal are consistent.

The AIM topological analysis (Supporting Information, Fig. S12) confirms all metal interactions with uracil, including the single interaction for $[\text{Zn}(\text{Ura-H})(\text{H}_2\text{O})_2]^+$, through the presence of BCPs. The positive nature of the Laplacian of the electron density, $\nabla^2\rho$, also confirms

the electrostatic nature of these interactions. The solvent coordination to the metals, as well as the hydrogen bonds between water and carbonyl, are also observed through the presence of BCPs.

3.4.1. Comparison of Computed and Experimental Spectra

The experimental spectra for $[M(\text{Ura-H})(\text{H}_2\text{O})_2]^+$ are compared to the spectra of the three lowest energy structures as determined by method 2 in Figure 8. For the Cu complex, remarkable agreement is obtained between the experimental spectrum and structure 2-i, allowing for confident assignment of structure 2-i as the principal contributor. Both the intensity as well as the scaled positions of the carbonyl stretching modes (1712 cm^{-1}), H_2O scissoring modes (1602 cm^{-1}), $\text{C}=\text{C}$ stretching mode (1533 cm^{-1}) and N-H wagging mode (1454 cm^{-1}) are in excellent alignment with the experimental spectrum. Another minor feature, C-H wagging at 1200 cm^{-1} , also matches between the experimental spectrum and structure 2-i. Though a case could be made for a contribution from structure 2-ii based on majority of the spectral features, it is the intense band at 1491 cm^{-1} , which corresponds to the H_2O scissoring in this isomer, which allows for this structure to be ruled out.

While the experimental spectrum for the Zn complex is not very well resolved, structure 2-ii still presents a compelling case. Even though there is a large band encompassing frequencies from approximately 1400 cm^{-1} to 1700 cm^{-1} , there are still local maxima that are evident that correspond to the scaled computed spectra for structure 2-ii. Of particular note, major bands in the spectrum for structure 2-ii occur at 1682 cm^{-1} , 1623 cm^{-1} , and 1457 cm^{-1} , corresponding to the hydrogen bonded carbonyl stretches, $\text{C}=\text{C}$ stretch and H_2O scissoring, respectively. These bands correspond to maxima observed within the broad band of the experimental spectrum. As was the case in for the Cu complex, the less intense C-H wagging vibration at 1200 cm^{-1} also corresponds

well. A more compelling argument, however, may be that structures 2-iv and 2-v are not only considerably higher in energy, but both contain an intense free carbonyl stretching frequency in their spectra ($\sim 1750\text{ cm}^{-1}$), which is absent in the experimental spectrum.

3.5. Computed Structures for $[\text{Zn}(\text{Ura-H})(\text{H}_2\text{O})_3]^+$

Using the 10 lowest energy isomers of $[\text{Zn}(\text{Ura-H})(\text{H}_2\text{O})_2]^+$ as a starting point, a total of 46 isomers were obtained for the triply hydrated Zn complex using computational method 1, all of which are given in Figure S9 (Supporting Information), with a comparison of energetics based upon method 2 for the five lowest energy structures. Based upon method number 2, the four lowest energy structures along with their computed energetics and spectra are presented in Figure 9. All structures demonstrate deprotonation of the uracil at the N3 position, which has been a consistent theme throughout. As we have seen with Zn previously, it does not participate in a bidentate interaction in this monomeric complex, instead binding directly to the N3 site. The lowest energy structure, labelled as structure 3-i, has all three solvent molecules bound directly to the metal center, two of which participate in a hydrogen bond to each of the neighbouring carbonyls. Both the single interaction between Zn and N3, as well as the hydrogen bonds between the water molecules and carbonyl positions are confirmed by the presence of BCPs in the AIM topological analysis (Figure S12).

The other structures presented in Fig 9 also have Zn bound solely to N3, but with only two water molecules bound to the metal center. However, in each case, the third water molecule hydrogen bonds to one of the water molecules linked directly to the metal. These structures are considerably higher in energy than structure 3-i.

3.5.1. Comparison of Computed and Experimental Spectra

The comparison between the experimental spectrum and the computed spectra of the lowest energy complexes is also given in Fig. 9. The experimental spectrum for the triply hydrated Zn complex is very similar to that for the doubly solvated complex in shape and resolution. The most prominent feature, carbonyl stretching at 1658 cm^{-1} , corresponds well to the calculated spectrum from structure 3-i. However, there is an absence of distinct bands in the experimental spectrum between 1430 cm^{-1} and 1530 cm^{-1} , a region with prominent bands in the spectra of each of the lowest energy structures. These bands, in the area of H_2O scissoring motion as well as N-H wagging, represent features that would be present regardless of the configuration of the complex. However, these motions are not obvious in the experimental spectrum, and although there are two minor bands near this region, their intensity is minimal. The calculated spectra of isomers 3-i, 3-iii and 3-iv are relatively consistent with the bands observed in the experimental spectrum above 1600 cm^{-1} , although both 3-iii and 3-iv are significantly higher in terms of relative energy.

4. Summary

The structures of $[\text{M}(\text{Ura-H})(\text{Ura})]^+$ as well as $[\text{M}(\text{Ura-H})(\text{H}_2\text{O})]^+$ where M corresponds to metal ions Cu^{2+} , Zn^{2+} , and Pb^{2+} , along with $[\text{M}(\text{Ura-H})(\text{H}_2\text{O})_2]^+$ for Cu^{2+} and Zn^{2+} , as well as $[\text{Zn}(\text{Ura-H})(\text{H}_2\text{O})_3]^+$, were examined using IRMPD spectroscopy in the $1000\text{--}1900\text{ cm}^{-1}$ mid-infrared region. Two different electronic structure calculation methods were employed for energy comparison of the various isomers, as well as for comparison with experimental spectra. There was good agreement between both computational methods for the structures and energetics. The IR spectra generated for these lowest energy structures also generally agreed best with the experimental IRMPD spectra in most cases, with some notable exceptions where assignment of a

structure could not be confidently made. $[\text{Cu}(\text{Ura-H})(\text{H}_2\text{O})]^+$ does not present adequate agreement between the experimental spectra and any of the computed spectra to allow for the assignment of a structure. Although experimental data in the O-H/N-H region was not collected, the calculated spectra of all lowest energy structures are identical in this region, and so no additional information could be gathered from this region in an attempt to assign the structures.

For all dimeric complexes, the lowest energy structures are deprotonated at N3 of uracil with the metal bound by a bidentate electrostatic interaction with N3 and O4, confirmed through AIM analysis. For hydrated monomeric species, the same pattern of deprotonation is observed, with the exception of $[\text{Cu}(\text{Ura-H})(\text{H}_2\text{O})]^+$ which is coordinated at the deprotonated N1 position. As this complex becomes doubly hydrated, the uracil is then deprotonated at N3, demonstrating a solvent effect in the Cu complexes. Though the $[\text{Zn}(\text{Ura-H})(\text{H}_2\text{O})]^+$ deprotonates at N3, the metal coordination is to O2 only, with the solvent transferring a proton to the uracil, resulting in $[\text{Zn}(\text{Ura})(\text{OH})]^+$, with the uracil moiety being a neutral keto-enol tautomer. Any water molecules present are bound to the metal ion and, for the most part, participate in hydrogen bonding with the neighbouring carbonyls, with the exception of $[\text{Cu}(\text{Ura-H})(\text{H}_2\text{O})]^+$ and $[\text{Zn}(\text{Ura})(\text{OH})]^+$ where no hydrogen bonding is observed. For the doubly and triply hydrated Zn species, metal coordination is monodentate to N3 only, while the water molecules are bound to Zn insert themselves between the metal and the neighbouring carbonyl groups for hydrogen bonding. The experimental spectrum of $[\text{Zn}(\text{Ura-H})(\text{H}_2\text{O})_3]^+$ does not contain many well defined spectral features, and as a result, multiple isomers are consistent with the bands that are experimentally observed.

5. Acknowledgements

The authors wish to thank the CLIO team (J.M. Ortega, C. Six, G. Perilhous, J.P. Berthet) as well as P. Maître and V. Steinmetz for their support during the experiments. The authors also acknowledge the computational resources provided by ACE-Net and Westgrid. Finally, T.D.F. acknowledges the financial contributions from NSERC, Canadian Foundation for Innovation, and Memorial University of Newfoundland.

6. References

1. J.D. Watson, F.H. Crick, *Nature*, **1953**, *171*, 737.
2. A.M. Pyle, *Science*, **1993**, *261*, 709.
3. V.K. Misra, D.E. Draper, *Biopolymers*, **1998**, *48*, 113.
4. E. Madore, C. Florentz, R. Giege, J. Lapointe, *J. Nucleic Acids Res.*, **1999**, *27*, 3583.
5. J.V. Burda, J. Sponer, J. Leszczynski, P. Hobza, *J. Phys. Chem. B*, **1997**, *101*, 9670.
6. P.O. Lowdin, *Rev. Mod. Phys.*, **1963**, *35*, 724.
7. M. Sabat, B. Lippert, *Met. Ions Biol. Syst.*, **1996**, *33*, 143.
8. M. Burkitt, *Methods Enzymol.*, **1994**, *234*, 66.
9. W. Bal, K.S. Kaprzak, *Toxicol Lett.*, **2002**, *127*, 55.
10. B. Halliwell, J.M.C. Gutteridge, *Arch. Biochim. Biophys. Acta*, **1986**, *246*, 501.
11. J.M. Berg, Y. Shi, *Science*, **1996**, *271*, 1081.
12. J.W.R. Schwabe, A. Klug, *Nat. Struct. Mol. Biol.*, **1994**, *1*, 345.
13. R.A. Goyer, H.G. Seiler, H. Sigel, A. Sigel, *Handbook on Toxicity of Inorganic Compounds*, Dekker, New York, NY, **1988**.

14. Y. Tsuchiya, T. Tamura, M. Fujii, M. Ito, *J. Phys. Chem.*, **1988**, *92*, 1760.
15. M.J. Scanlan, I.H. Hillier, *J. Am. Chem. Soc.*, **1984**, *106*, 3737.
16. M. Piacenza, S. Grimme, *J. Comput. Chem.*, **2004**, *25*, 83.
17. J.K. Wolken, F. Turecek, *J. Am. Soc. Mass Spectrom.*, **2000**, *11*, 1065.
18. E.S. Kryachko, M.T. Nguyen, T. Zeegers-Huyskens, *J. Phys. Chem. A*, **2001**, *105*, 1288.
19. E. Rincón, M. Yañez, A. Toro-Labbé, O. Mo, *Phys. Chem. Chem. Phys.*, **2007**, *9*, 2531.
20. S. Guillaumont, J. Tortajada, J.Y. Salpin, A.M. Lamsabhi, *Int. J. Mass Spectrom.*, **2005**, *243*, 279.
21. T. Marino, D. Mazzuca, M. Toscano, N. Russo, A. Grand, *Int. J. Quantum Chem.*, **2007**, *107*, 311.
22. O.Y. Ali, T.D. Fridgen, *Int. J. Mass Spectrom.*, **2011**, *308*, 167.
23. O.Y. Ali, N.M. Randell, T. D. Fridgen, *ChemPhysChem*, **2012**, *13*, 1507.
24. A.A. Power, O.Y. Ali, M.B. Burt, T.D. Fridgen, *Int. J. Mass Spectrom.*, **2012**, *330–332*, 233.
25. B. Power, V. Haldys, J.-Y. Salpin and T.D. Fridgen, *Int. J. Mass Spectrom.*, **2015**, *378*, 328.
26. B. Power, V. Haldys, J.-Y. Salpin and T.D. Fridgen, *J. Mass Spectrom.*, **2016**, *51*, 236.
27. A.M. Lamsabhi, M. Alcamí, M. Otilia, M. Yañez, J. Tortajada, *J. Phys. Chem. A*, **2006**, *110*, 1943.
28. A.M. Lamsabhi, M. Alcamí, O. Mó, M. Yañez, J. Tortajada, J.-Y. Salpin, *ChemPhysChem*, **2007**, *8*, 181.
29. O.Y. Ali, T.D. Fridgen, *ChemPhysChem*, **2012**, *13*, 588.
30. B. Power, S.A. Rowe, T.D. Fridgen, *J. Phys. Chem. B*, **2017**, *121*, 58.
31. R. Prazeres, F. Glotin, C. Insa, D.A. Jaroszynski, J.M. Ortega, *Eur. Phys. J. D: At., Mol., Opt. Plasma Phys.*, **1998**, *3*, 87.

32. W. Paul, *Rev. Mod. Phys.*, **1990**, *62*, 531.
33. K. Rajabi, M.L. Easterling, T.D. Fridgen, *J. Am. Soc. Mass Spectrom.*, **2009**, *20*, 411.
34. M.J. Frisch, G.W. Trucks, H.B. Schlegel, G.E. Scuseria, M.A. Robb, J.R. Cheeseman, G. Scalmani, V. Barone, B. Mennucci, G.A. Petersson, H. Nakatsuji, M. Caricato, X. Li, H.P. Hratchian, A.F. Izmaylov, J. Bloino, G. Zheng, J.L. Sonnenberg, M. Hada, M. Ehara, K. Toyota, R. Fukuda, J. Hasegawa, M. Ishida, T. Nakajima, Y. Honda, O. Kitao, H. Nakai, T. Vreven, J.A. Montgomery, J.E. Peralta J., F. Ogliaro, M. Bearpark, J.J. Heyd, E. Brothers, K.N. Kudin, V.N. Staroverov, T. Keith, R. Kobayashi, J. Normand, K. Raghavachari, A. Rendell, J.C. Burant, S.S. Iyengar, J. Tomasi, M. Cossi, N. Rega, J.M. Millam, M. Klene, J.E. Knox, J.B. Cross, V. Bakken, C. Adamo, J. Jaramillo, R. Gomperts, R.E. Stratmann, O. Yazyev, A.J. Austin, R. Cammi, C. Pomelli, J.W. Ochterski, R.L. Martin, K. Morokuma, V.G. Zakrzewski, G.A. Voth, P. Salvador, J.J. Dannenberg, S. Dapprich, A.D. Daniels, O. Farkas, J.B. Foresman, J.V. Ortiz, J. Cioslowski, D.J. Fox, *Gaussian 09*, Revision D.01, Gaussian, Inc., Wallingford, CT, **2013**.
35. P.B. Armentrout, M. Citir, Y. Chen, M.T. Rodgers, *J. Phys. Chem. A*, **2012**, *116*, 11823.
36. P.B. Armentrout, Y. Chen, M.T. Rodgers, *J. Phys. Chem. A*, **2012**, *116*, 3989.
37. R.F.W. Bader, *Atoms in Molecules: A Quantum Theory*, Clarendon Press, Oxford University Press, New York, NY, **1990**.
38. T.A. Keith, AIMAll, Version 14.10.27, TK Gristmill Software, Overland Park, KS, 2014, aim.tkgristmill.com.
39. P. Colarusso, K. Zhang, B. Gup, P.F. Bernath, *Chem. Phys. Lett.*, **1997**, *269*, 39.
40. J.-W. Shin, *Int. J. Mass Spectrom.*, **2014**, *372*, 39.
41. J.-Y. Salpin, V. Haldys, S. Guillaumont, J. Tortajada, M. Hurtado, A.M. Lamsabhi, *ChemPhysChem*, **2014**, *15*, 2959.
42. S.J. Lippard, J.M. Berg, *Principles of Bioinorganic Chemistry*, University Science Books, Mill Valley, CA, **1994**.
43. W. Kaim, B. Schwedersky, *Bioinorganic Chemistry Inorganic Elements in the Chemistry of Life*, John Wiley & Sons, Chichester, UK, **1994**.

44. L.A. Loeb, A.R. Zakour, *Nucleic Acids-Metal Ion Interactions*, T.G. Spiro Ed., John Wiley & Sons, New York, NY, **1980**.

45. D.W. Christianson, J.D. Cox, *Annu. Rev. Biochem.*, **1999**, 68, 33.

Figure Captions

Scheme 1. Numbering scheme for uracil.

Figure 1. Infrared multiple photon dissociation spectra for $[M(\text{Ura-H})(\text{Ura})]^+$ ($M = \text{Cu}, \text{Zn}, \text{Pb}$) in the 1000–1900 cm^{-1} region.

Figure 2. Infrared multiple photon dissociation spectra for $[M(\text{Ura-H})(\text{H}_2\text{O})]^+$ ($M = \text{Cu}, \text{Zn}, \text{Pb}$) in the 1000–1900 cm^{-1} region.

Figure 3. Infrared multiple photon dissociation spectra for $[\text{Zn}(\text{Ura-H})(\text{H}_2\text{O})_2]^+$, $[\text{Cu}(\text{Ura-H})(\text{H}_2\text{O})_2]^+$ and $[\text{Zn}(\text{Ura-H})(\text{H}_2\text{O})_3]^+$ in the 1000–1900 cm^{-1} region.

Figure 4. Comparison of the energies and structures for the lowest energy $[M(\text{Ura-H})(\text{Ura})]^+$ complexes, $M = \text{Cu}, \text{Zn}, \text{Pb}$. The thermochemistry reported here are those from method 2.

Figure 5. Experimental IRMPD spectrum (bottom) for $[M(\text{Ura-H})(\text{Ura})]^+$ compared with the B3LYP computed spectra using computational method 2 for the lowest energy structures. The calculated relative enthalpies and 298 K Gibbs energies (*italics*) are also shown.

Figure 6. Comparison of the energies and structures for the lowest energy $[M(\text{Ura-H})(\text{H}_2\text{O})]^+$ complexes, $M = \text{Cu}, \text{Zn}, \text{Pb}$. The thermochemistry reported here are those from method 2.

Figure 7. Experimental IRMPD spectrum (bottom) for $[M(\text{Ura-H})(\text{H}_2\text{O})]^+$ compared with the B3LYP computed spectra using computational method 2 for the lowest energy structures. The calculated relative enthalpies and 298 K Gibbs energies (*italics*) are also shown.

Figure 8. Experimental IRMPD spectrum (bottom) for $[M(\text{Ura-H})(\text{H}_2\text{O})_2]^+$, $M = \text{Cu}$ (left) and Zn (right), compared with the B3LYP computed spectra using computational method 2 for the three lowest energy structures. The calculated relative enthalpies and Gibbs energies (*italics*) are also shown.

Figure 9. Experimental IRMPD spectrum (bottom) for $[\text{Zn}(\text{Ura-H})(\text{H}_2\text{O})_3]^+$, compared with the B3LYP computed spectra using computational method 2 for the four lowest energy structures. Isomer 3-i is also shown rotated 90° clockwise about a vertical axis. The calculated relative enthalpies and Gibbs energies (*italics*) are also shown.

Keywords

- IRMPD spectroscopy;
- Metal cation;
- Uracil;
- DNA base;
- Ion–molecule complex

Highlights

- Structures of bare M-Ura dimers and M-Ura monomers (M = Cu, Zn, Pb) were studied via IRMPD spectroscopy and DFT calculations.
- In dimers, one uracil is deprotonated at N3 with tetracoordinate binding of the metal to N3 and O4 of Ura-H and N3 and O2 of Ura.
- Monomers generally deprotonate at N3, however a solvent effect is observed in the tautomerization of uracil in Cu complexes.
- Proton transfer occurs in $[\text{Zn}(\text{Ura-H})(\text{H}_2\text{O})]^+$ from water to uracil, resulting in a neutral keto-enol uracil tautomer.

Scheme 1

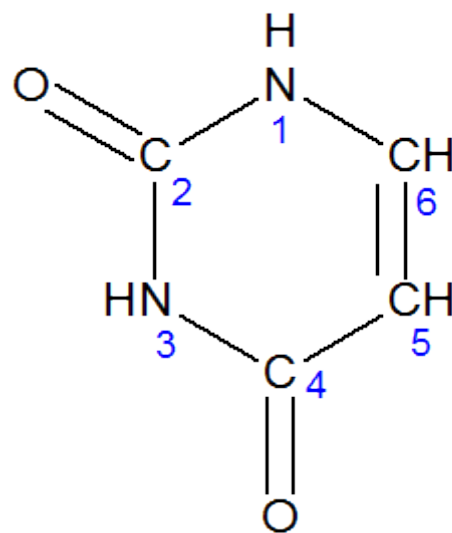


Figure 1

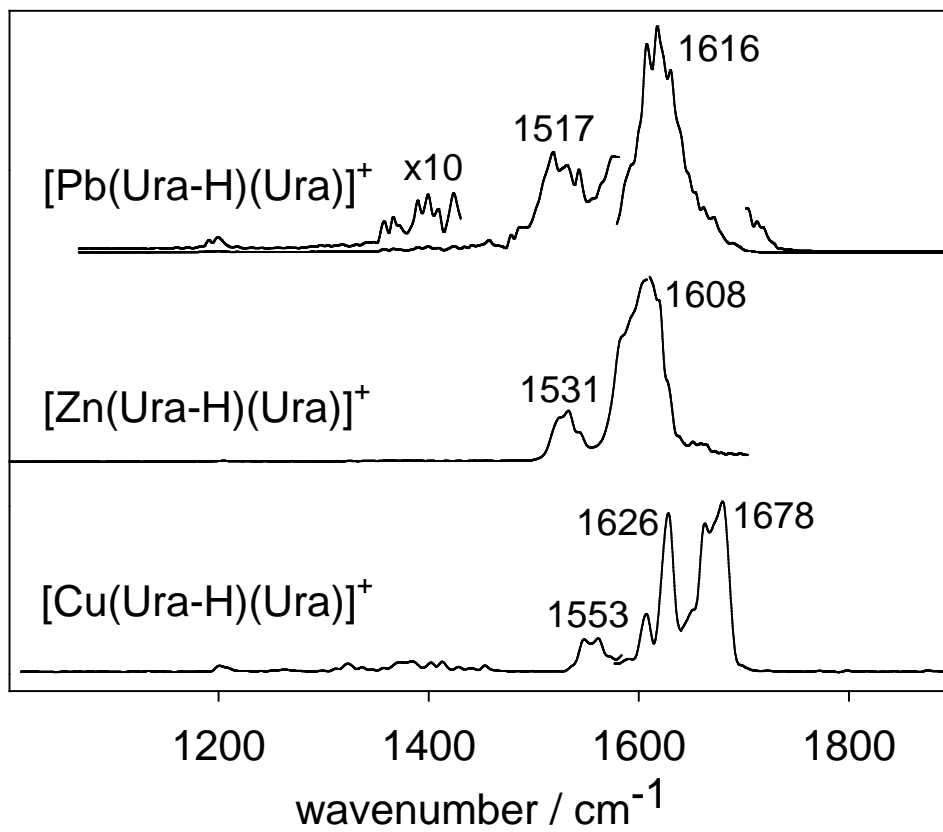


Figure 2

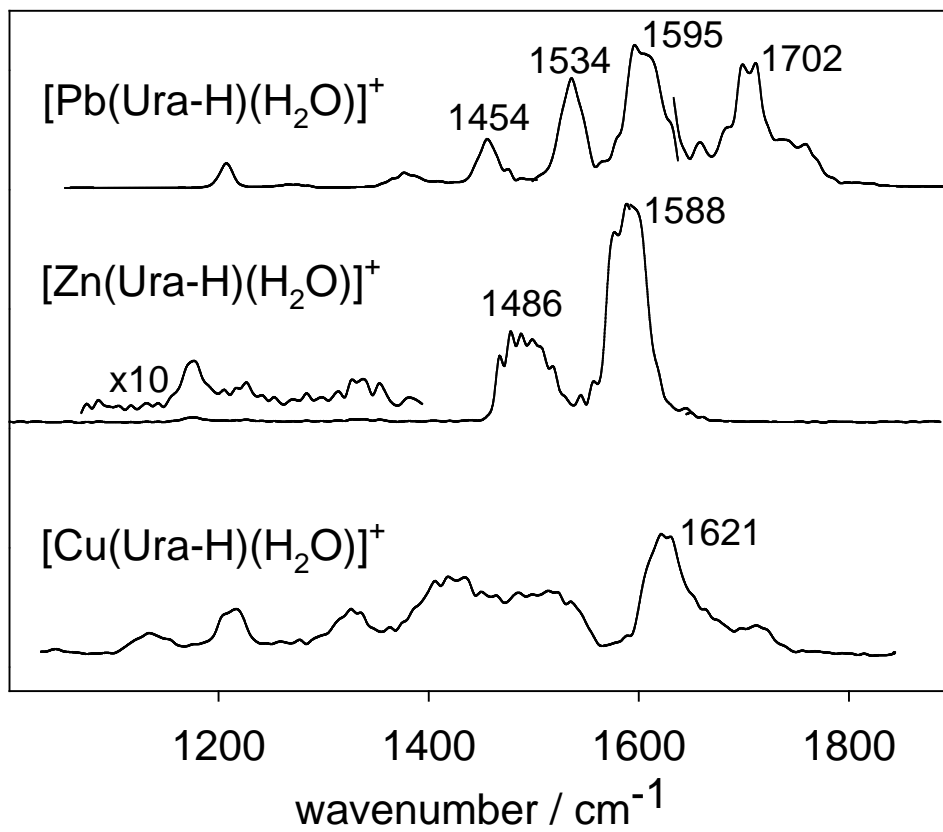


Figure 3

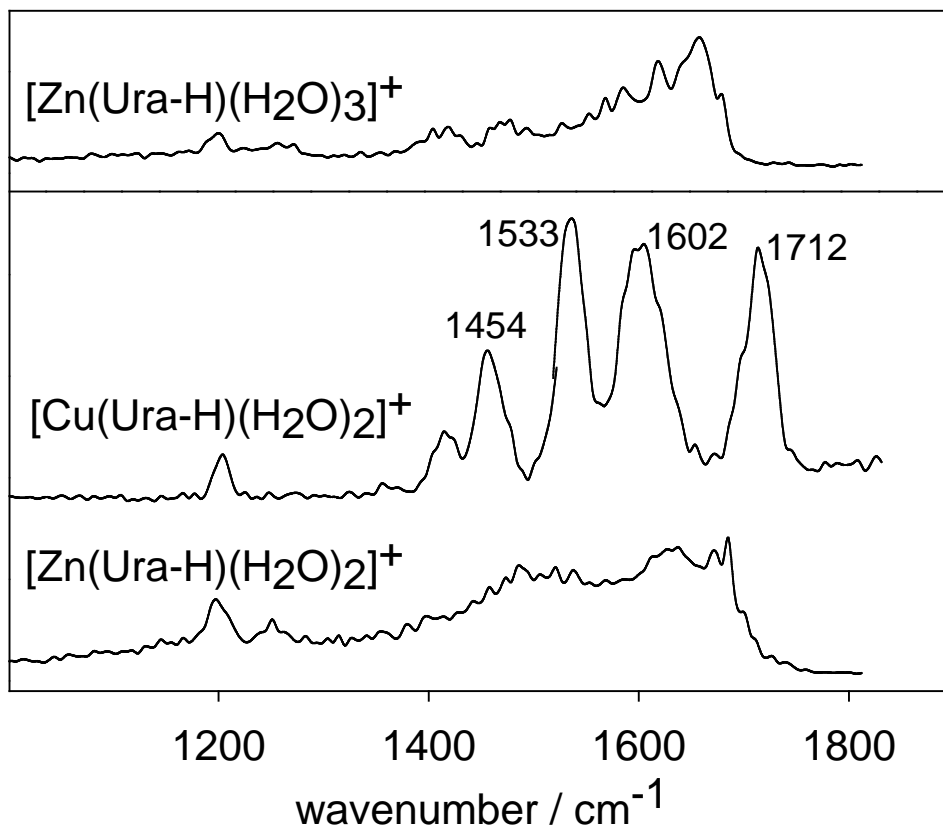
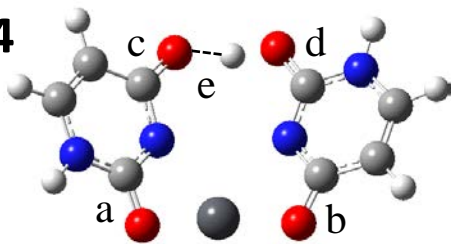


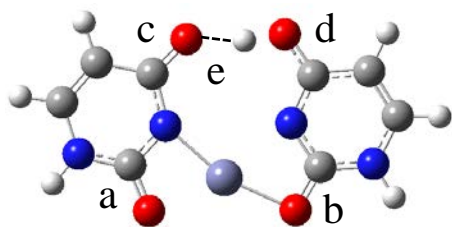
Figure 4

iv



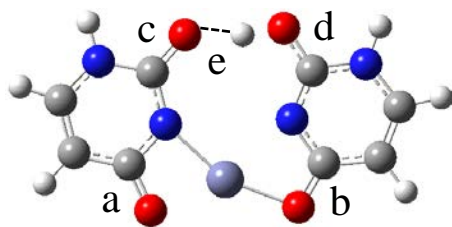
M	$\Delta_{\text{rel}}H/\Delta_{\text{rel}}G$	a	b	c	d	e
Pb	8.5/8.6	1.268	1.269	1.258	1.285	1.373

iii



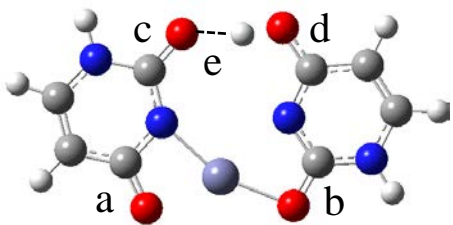
M	$\Delta_{\text{rel}}H/\Delta_{\text{rel}}G$	a	b	c	d	e
Pb	8.8/8.9	1.270	1.263	1.248	1.294	1.509
Zn	12.7/12.2	1.273	1.277	1.248	1.288	1.487
Cu	7.6/7.4	1.274	1.263	1.248	1.284	1.452

ii



M	$\Delta_{\text{rel}}H/\Delta_{\text{rel}}G$	a	b	c	d	e
Pb	3.4/4.1	1.276	1.267	1.250	1.295	1.475
Zn	0.0/0.0	1.280	1.281	1.249	1.289	1.460
Cu	1.8/2.3	1.278	1.267	1.250	1.285	1.435

i



M	$\Delta_{\text{rel}}H/\Delta_{\text{rel}}G$	a	b	c	d	e
Pb	0.0/0.0	1.278	1.262	1.244	1.299	1.566
Zn	1.3/0.7	1.281	1.277	1.243	1.293	1.543
Cu	0.0/0.0	1.282	1.261	1.243	1.290	1.526

Figure 5

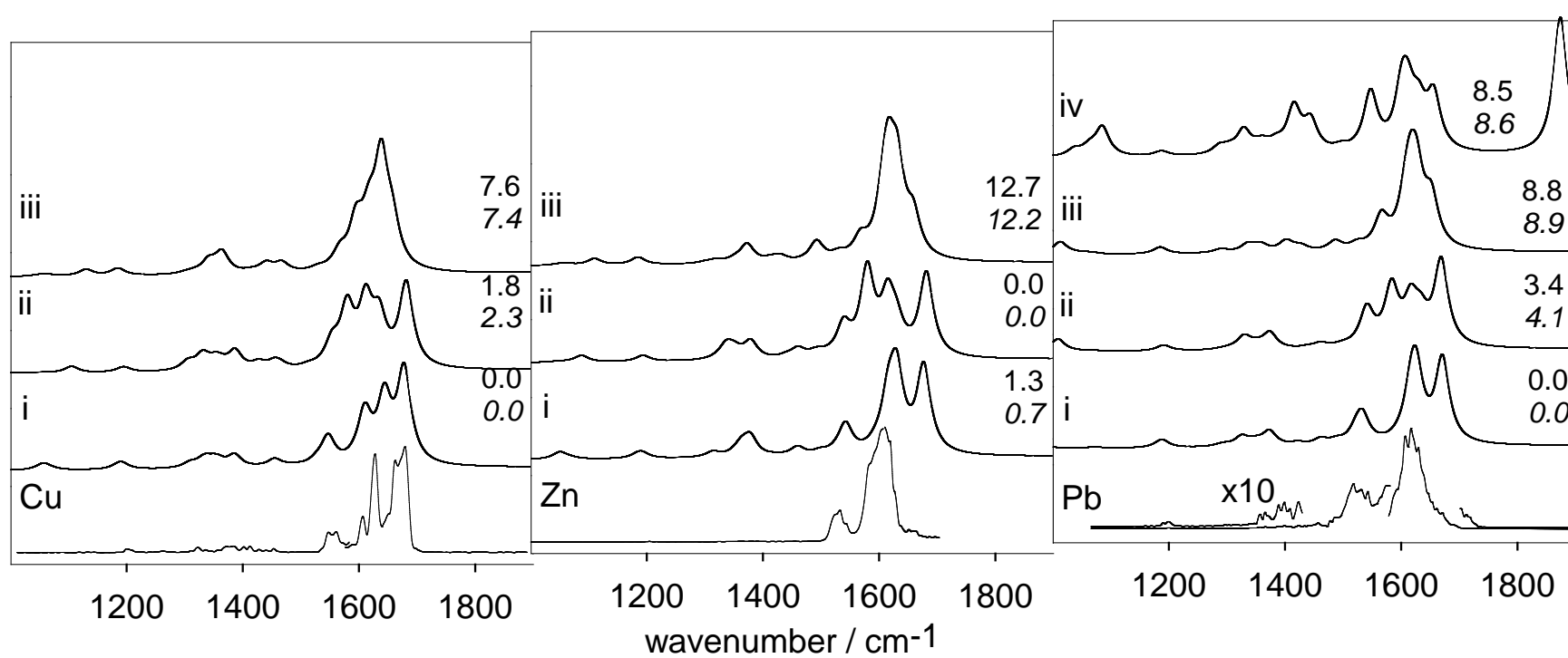


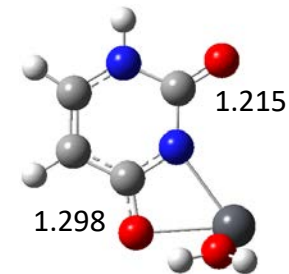
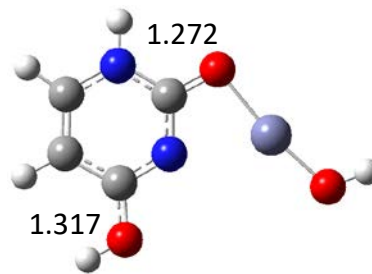
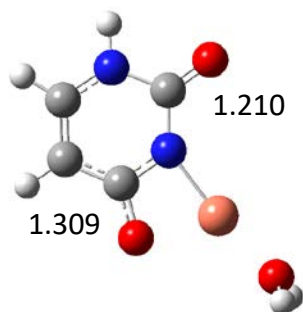
Figure 6

Cu

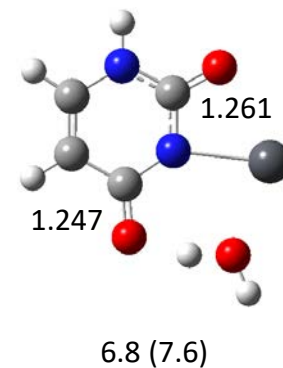
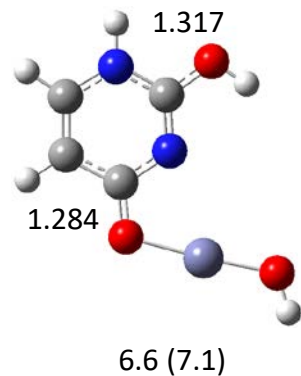
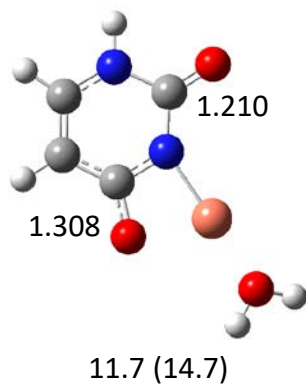
Zn

Pb

1-iii



1-ii



1-i

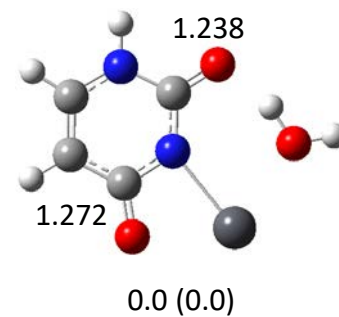
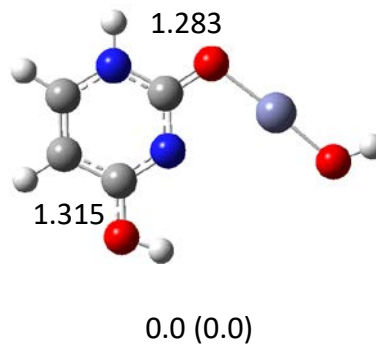
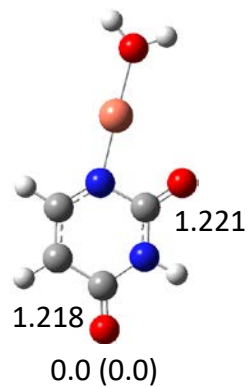


Figure 7

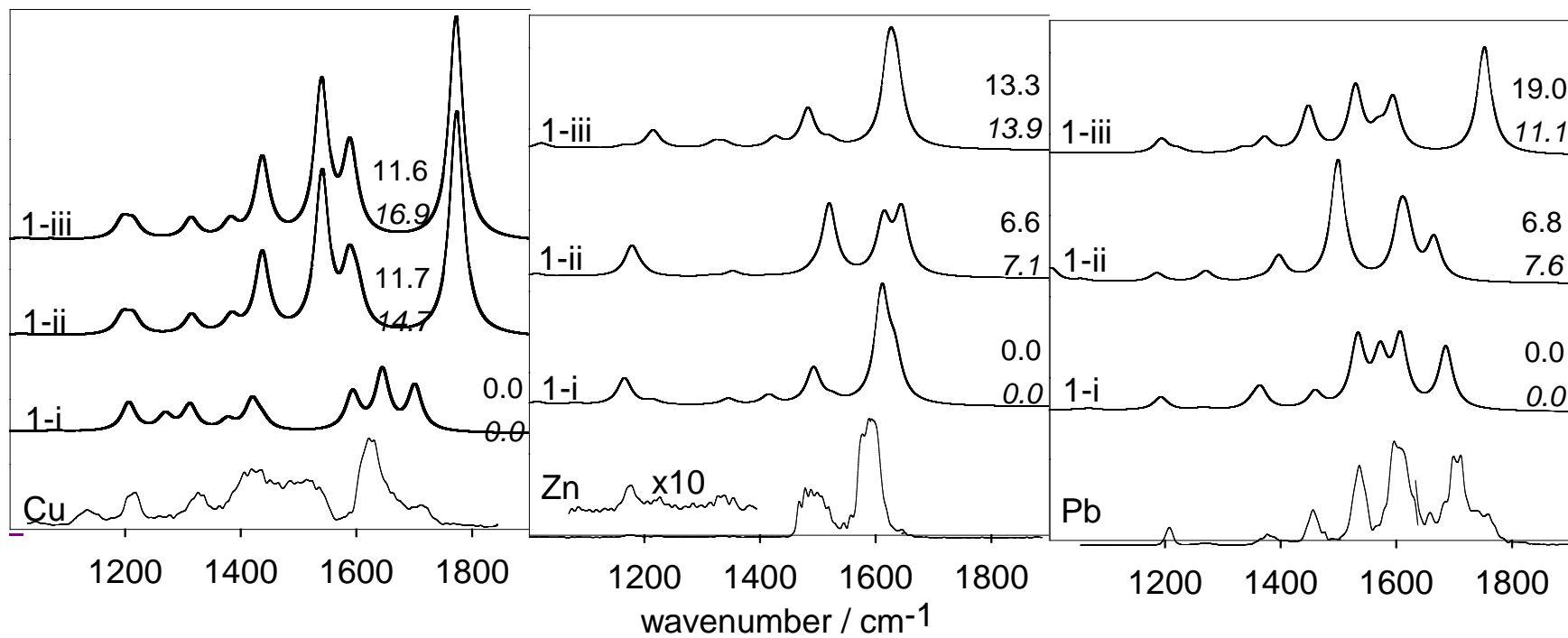


Figure 8

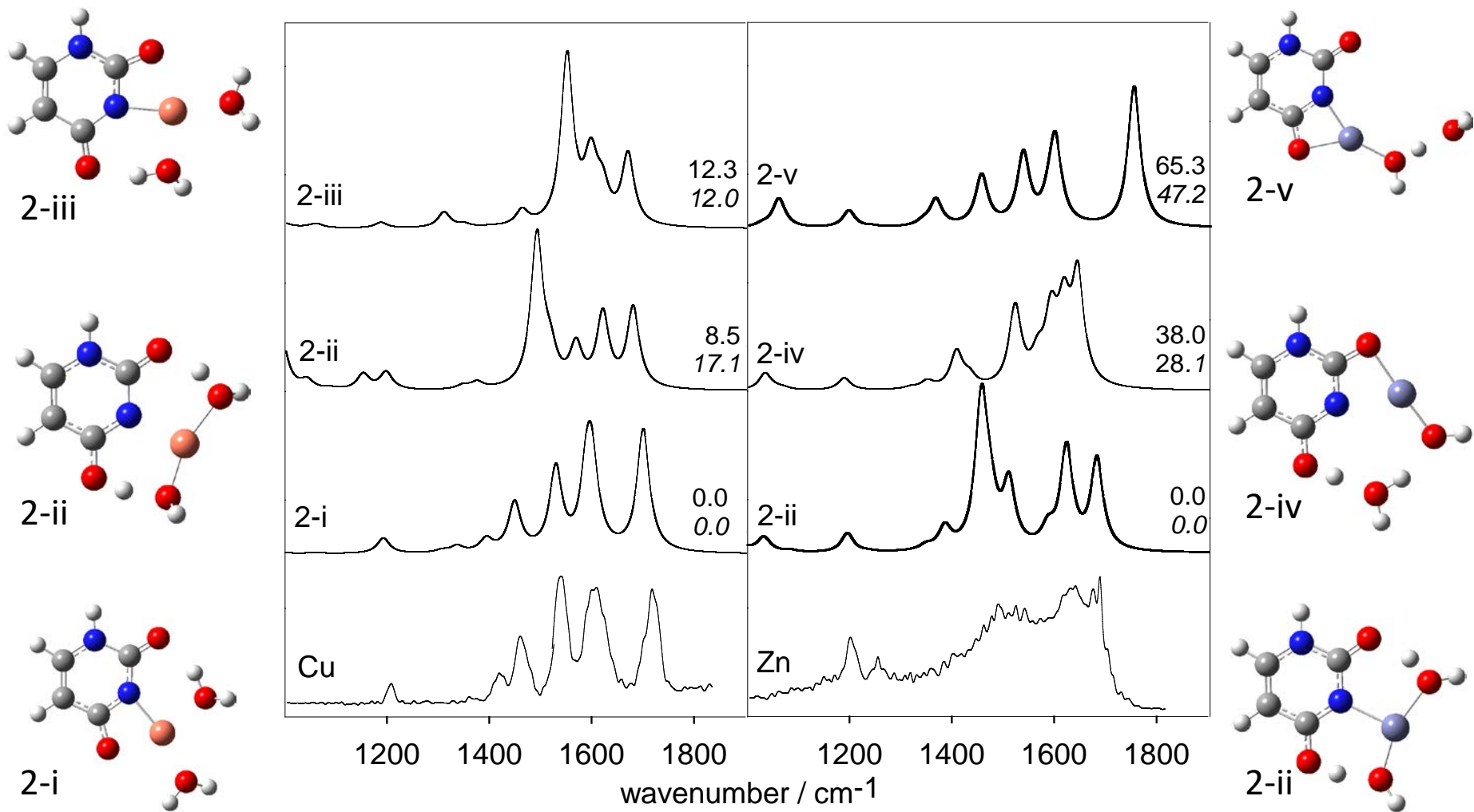
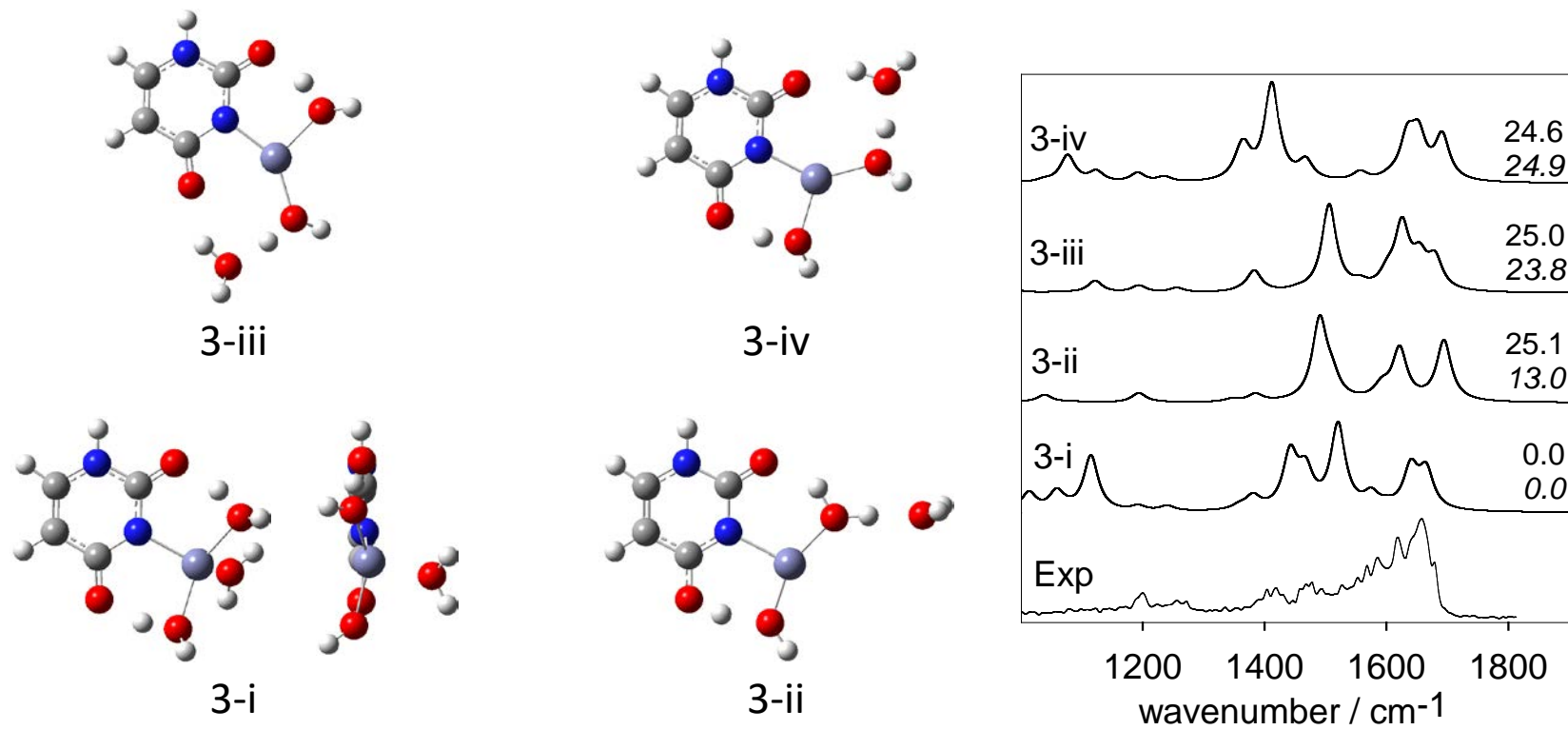


Figure 9



Graphical Abstract

